

VOID GROWTH IN SINGLE AND BICRYSTALLINE METALS: ATOMISTIC CALCULATIONS

Sirirat Traiviratana*, Eduardo M. Bringa[†], David J. Benson* and Marc A. Meyers*

**Dept. of Mech. and Aerospace Engr., Univ. of California, San Diego, La Jolla, CA 92093, USA*

[†]*Materials Science Department, Lawrence Livermore National Laboratory, Livermore, CA 94550, USA*

Abstract. MD simulations in monocrystalline and bicrystalline copper were carried out with LAMMPS to reveal void growth mechanisms. The specimens were subjected to both tensile uniaxial and hydrostatic strains; the results confirm that the emission of (shear) loops is the primary mechanism of void growth. However, these shear loops develop along two slip planes (and not one, as previously thought), in a heretofore unidentified mechanism of cooperative growth. The emission of dislocations from voids is the first stage, and their reaction and interaction is the second stage. These loops, forming initially on different $\{111\}$ planes, join at the intersection, the Burgers vector of the dislocations being parallel to the intersection of two $\{111\}$ planes: a $\langle 110 \rangle$ direction. Thus, the two dislocations cancel at the intersection and a biplanar shear loop is formed. The expansion of the loops and their cross slip leads to the severely work hardened layer surrounding a growing void. Calculations were carried out on voids with different sizes, and a size dependence of the stress response to emitted dislocations was observed, in disagreement with the Gurson model[1] which is scale independent. Calculations were also carried out for a void at the interface between two grains.

Keywords: void, growth, copper, single, bi, nano, crystal, atomistic

PACS: 02.70.Ns, 07.05.Tp

INTRODUCTION

Fracture of ductile metals occurs by nucleation, growth and coalescence of voids[2]. There have been a number of proposed continuum models for the growth of voids in both two and three dimensions[1, 3, 4]. However, until recently there was no well established atomistic mechanism for void growth, and the model proposed by Cuitiño and Ortiz[5] is based on vacancy pipe diffusion. Lubarda et al.[6] demonstrated that the vacancy diffusion mechanism is only applicable at low strain rates and/or high temperatures, and is therefore only relevant in creep deformation. Failure in creep is preceded by void nucleation and growth at the grain boundaries and has been successfully modeled using the diffusion equation by Raj and Ashby[7]. The regime encountered in laser compression is radically different, with strain rates on the order of 10^6 s^{-1} and higher.

Analytical results by Lubarda et al.[6] and molecular dynamics simulations by Rudd and coworkers[8–11] and Marian, Knapp and Ortiz[12, 13] indicate that dislocation emission from the growing voids is the primary mechanism of radial material transfer required for expansion. Both prismatic and shear loops were postulated[6] and observed in MD simulations[8–14]. It is the objective of this report to analyze the growth of voids in greater detail. The grain boundary nature and void size were altered to examine their effect on growth mechanisms.

EXPERIMENTAL OBSERVATION

Dislocation activity around a void growing in the spall regime of shock compressed copper was reported by Meyers and Aimone[15] and Christy et

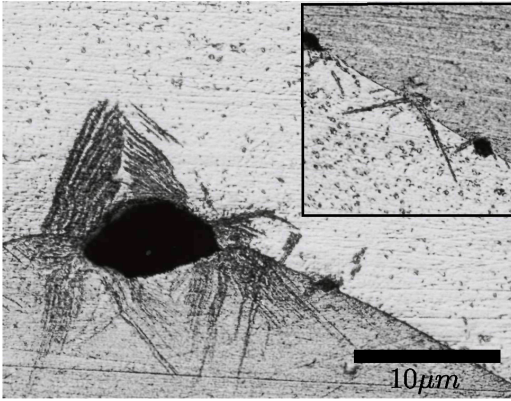


FIGURE 1. Evidence of slip around growing voids.

al.[16]. Fig.1 shows slip bands emanating from voids that nucleated at grain boundaries in copper. However, the exact nature of dislocation generation and evolution cannot be obtained from these observations. This requires detailed analysis methods such as MD.

COMPUTATIONAL APPROACH

The molecular dynamics LAMMPS (Large-scale Atomic/Molecular Massively Parallel Simulator)[17] code was used in this investigation. For the FCC copper structure an EAM[18] Mishin[19] potential was used. The number of atoms was varied from 10^5 to 10^7 , and calculations were performed on parallel PCs and supercomputer at San Diego Super Computer Center.

The single crystal copper domain was $10 \times 10 \times 10 \text{ nm}$ with 1 nm radius spherical void at center. This gives a void volume fraction of 0.42%. A periodic boundary was used with two types of loading: hydrostatic expansion strain and uniaxial expansion strain. The domain size was also reduced to 0.5 nm radius void and enlarged to 2.0 nm radius void while fixing void volume fraction at 0.42%. The different sized domains were subjected to uniaxial strain along $[001]$. All simulations were done at a strain rate of 10^8 s^{-1} (2000 picoseconds, 20% volume strain). Visualization of stacking faults representing dislocations was done with a filter using a centrosymmetry parameter[20]. A bicrystal

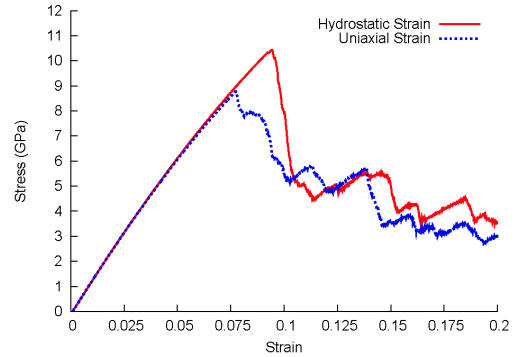


FIGURE 2. Stress-strain relations for uniaxial strain against hydrostatic strain loading for 1 nm void radius.

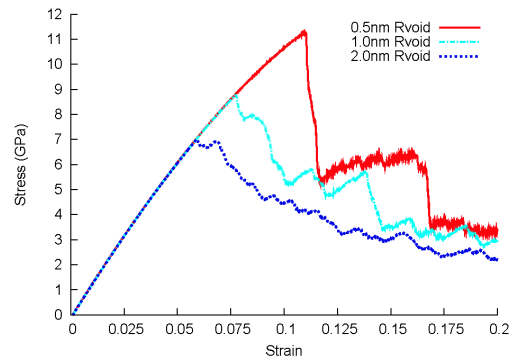


FIGURE 3. Stress-strain relations for different void sizes, showing size-scale dependence of yield stress.

copper domain was constructed with two single crystal cubes sharing a tilt boundary, $\theta = 43.6^\circ$. The domain underwent annealing and relaxation to minimize grain boundary energy; a spherical void was cut followed by a second relaxation to minimize void surface energy. Uniaxial volume strain was applied at a strain rate of $5 \times 10^9 \text{ s}^{-1}$.

RESULTS

Hydrostatic and uniaxial strain simulations show a difference in the yield stress (the stress at which the voids start growing); the yield stress for uniaxial strain was lower, Fig.2. This difference is due to the fact that the shear stresses resulting from hydrostatic

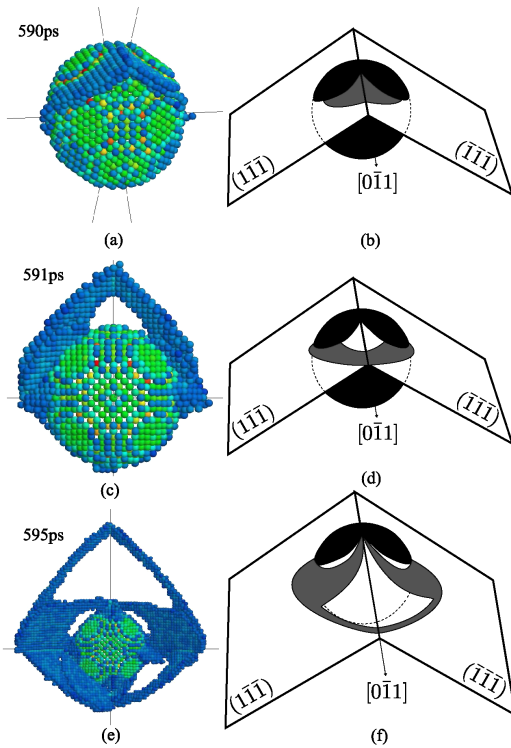


FIGURE 4. Sequences of loop nucleation and growth, (2.0nm radius void; uniaxial strain)(Rendered atoms and their sketched counterparts).

strain are considerably lower than in the case of uniaxial strain. An additional, but related, effect is that the formation of dislocations under hydrostatic strain was generally more complex.

The size-scale dependence of yield stress can be observed in uniaxial strain simulations with various sizes of domains, Fig.3. The void fraction was kept constant at 0.42%. As the void size increases, the yield stress drops: it is 11GPa for 0.5nm and 7GPa for 2nm void. This is in opposition to the Gurson criterion, which is size independent. The formation of loops in uniaxial strain loading is more consistent and easier to study than in hydrostatic loading, Fig.4.

Fig.4 shows both the MD simulations(left) and models for generation and propagation of dislocations(right) at increasing times. Shear loops on different $\{111\}$ planes connect at the $\langle 110 \rangle$ intersection (Figs.4a,b), then extend away from void (Figs.4c,d).

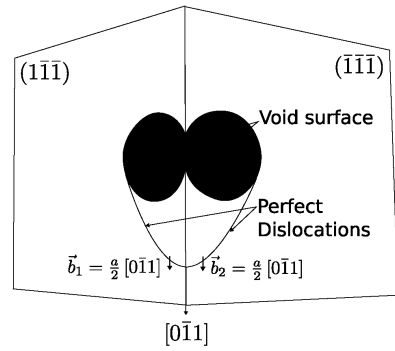


FIGURE 5. Top view of two perfect dislocations.

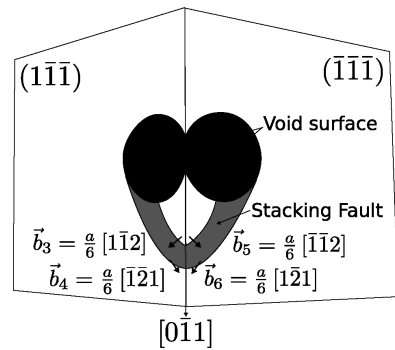


FIGURE 6. Top view of partial dislocations.

As the leading partial expands, the trailing partial follows it. More complex dislocation interactions take place as the shear loops propagate outwards (Figs.4e,f).

In general the stacking fault consists of two layers of atoms composing the plane of the dislocation. When an additional layer forms itself on top of these two layers, the plane opens up with trailing edge of dislocation closing the stacking fault. At this point, it becomes a shear loop with a narrow stacking fault band. Shear loops continue to travel outward from the void surface as they transport material, accommodating the growth of void.

Dislocation planes are of the family $\{111\}$. Partial dislocations on two planes interact at the initiation stage, forming an angle in which they tie and travel together as they expand. This interaction happens for any two partial dislocation planes that nucleate next

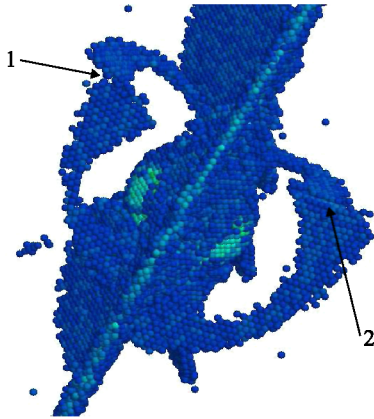


FIGURE 7. Shear loops and interaction in bicrystals simulation with uniaxial strain.

to each other, Fig.4.

A more detailed dislocation analysis is shown in Figs.5 (perfect dislocations) and 6 (partial dislocations). In Fig.5, two perfect dislocation loops, \vec{b}_1 and \vec{b}_2 , forming on (111) and $(\bar{1}\bar{1}\bar{1})$, respectively, interact from the early state of dislocation formation. They have parallel Burgers vectors but are on different planes. The intersection line is also aligned with $[011]$ which allows the two dislocations to glide without forming sessile segments. Actually, they cancel each other at the $\langle 110 \rangle$ intersection.

The interaction of perfect dislocations can be extended to partial dislocations (Fig.6). The leading partials \vec{b}_4 and \vec{b}_6 react and form a sessile dislocation $\frac{a}{3}[100]$; the trailing partials form an opposite dislocation $\frac{a}{3}[100]$. They cancel each other as the partials move, leaving the crystalline structure undistorted behind. The $\frac{a}{3}[100]$ dislocation is sessile and has an energy below the $\vec{b}_4 + \vec{b}_6$ sum. It constricts the loop at the slip-plane intersection. Hence, the biplanar shear loop mechanism is applicable to the case where perfect dislocations decompose into partials. This is also clearly seen in the simulation of Fig.4c. It should be noted that dislocation reactions should be: $\vec{b}_1 - \vec{b}_2$ (and, accordingly, $\vec{b}_3 - \vec{b}_5$ and $\vec{b}_4 - \vec{b}_6$) because of the dislocation loop line vectors in the (111) and $(\bar{1}\bar{1}\bar{1})$ which are opposed.

Bicrystal simulation, although done at much higher strain rate ($5 \times 10^9 \text{ s}^{-1}$) shows results consistent with single crystal void growth. Partial

dislocation loops are emitted from the void surface, interact and travel together as the strain increases, Fig.7. One can see at least two biplanar shear loops emanating from the void in Fig.7 (marked 1 and 2), one in each grain. The dislocation interactions are more complex because the number of slip planes involved is twice as high. The results presented here are only preliminary, and several parameters for bicrystal orientation are being varied to allow the extraction of more meaningful results.

Acknowledgements. Financial support from LLNL grant B558558 and ILSA contract number W-7405-Eng-48 is gratefully acknowledged.

REFERENCES

1. Gurson, A., *J.Engr.Mater.Tech.*, **99**, 2 (1977).
2. McClintock, F., Argon, A., Backer, S., and Orowan, E., *Mechanical Behavior of Materials*, A.W., 1966.
3. Needleman, A., and Tvergaard, V., *J.Mech.Phys.Solids.*, **32**, 461 (1984).
4. Tvergaard, V., and Needleman, A., *Acta Mat.*, **32**, 157 (1984).
5. Cuitiño, A., and Ortiz, M., *Acta Mat.*, **44**, 863 (1996).
6. Lubarda, V., Schneider, M., Kalantar, D., Remington, B., and Meyers, M., *Acta Mat.*, **53**, 1397 (2004).
7. Raj, R., and Ashby, M., *Acta Met.*, **23**, 653 (1975).
8. Rudd, R., and Belak, J., *Co.Mat.Sci.*, **24**, 148 (2002).
9. Seppälä, E., Belak, J., and Rudd, R., *Phys.Rev.B*, **69**, 1 (2004).
10. Seppälä, E., Belak, J., and Rudd, R., *PRL*, **93**, 1 (2004).
11. Seppälä, E., Belak, J., and Rudd, R., *Phys.Rev.B*, **71**, 1 (2005).
12. Marian, J., Knap, J., and Ortiz, M., *PRL*, **93**, 1 (2004).
13. Marian, J., Knap, J., and Ortiz, M., *Acta Mat.*, **53**, 2893 (2005).
14. Ahn, D., Sofronis, P., Kumar, M., Belak, J., and Minich, R., *J.Appl.Phys.*, **101**, 063514 (2007).
15. Meyers, M., and Aifone, C., *P.M.S.*, **28** (1983).
16. Christy, S., Pak, H.-r., and Meyers, M., *Metallurgical Applications of Shock Wave and High-Strain-Rate Phenomena*, Dekker, New York, eds, 1986.
17. Plimpton, S., *J. Comp. Phys.*, **117**, 1 (1995), <http://lammps.sandia.gov>.
18. Daw, M., and Baskes, M., *Phys.Rev.B*, **29**, 6443 (1984).
19. Mishin, Y., Mehl, M., Papaconstantopoulos, D., Voter, A., and Kress, J., *Phys.Rev.B*, **63**, 224106 (2001).
20. Kelchner, C., Plimpton, S., and Hamilton, J., *Phys.Rev.B*, **58**, 11085 (1998).